MODELING DUCTILE DAMAGE OF STEEL IN AGGRESSIVE ENVIRONMENT

ROBERT KUCHARSKI

The Szewalski Institiute of Fluid-flow Machinery, Polish Academy of Sciences
Fiszera 14, 80-952 Gdansk, Poland
robertk@imp.gda.pl

(Received 8 September 2006; revised manuscript received 29 September 2006)

Abstract: This paper is a proposition of a new damage model, extended to include the influence of the external environment, based on the Gurson yield function and a new damage evolution equation. The model also contains a mass transport equation based on Fick's law. A comparison of experimental and numerical results is included.

Keywords: stress corrosion damage, reaction-diffusion equations, damage evolution equation, FEM

1. Introduction

In order to determine whether a material is damaged it may be necessary to study its cleavage, ductility, fracture, creep, fatigue and corrosion. Local models can be formulated for cleavage [1], creep [2–5] and low-cycle fatigue. Ductile fracture has received considerable attention since the initial study [6] that first recognized the formation and growth of microvoids as the governing mechanism of rapture. Since then, a number of papers have been published addressing both experimental and modeling issues. Ductile damage is described in terms of void volume fraction ω that affects a material's plastic potential at the macroscale by means of a softening term. The damage evolution law is developed from the study of a single isolated cavity in "virgin", undamaged material. In this context Rice and Tracy [6] proposed thrir relation for the cavity growth rate. A modified yield criterion for ductile metals with increasing porosity was derived later in [7]. Void nucleation was incorporated into the Gurson model by Needleman [8] and adopted to creep damage by Bielecki [4]. Against this background, the author of this paper has decided to add the influence of the external environment to the well-known Gurson-Needelman model. Numerous experimental results have shown that aspect or external influence cannot be neglected and is one of the main factors resulting in material damage [9–13]. Similar results can be found in [14–16].

2. Governing equations of the general theory

The model consists of two parts: the mechanical and the difussion-reaction part.

2.1. Mechanical

We confine ourselves to a situation in which the deformation rate, $\dot{\varepsilon}_{ij}$, is a sum of the elastic and plastic parts:

$$\dot{\varepsilon}_{ij} = \dot{\varepsilon}_{ij}^{\mathrm{el}} + \dot{\varepsilon}_{ij}^{\mathrm{pl}}. \tag{1}$$

The elastic part of a strain tensor is definied as [6]:

$$\varepsilon_{ij}^{\mathrm{el}} = \frac{1+\nu^{\mathrm{eff}}}{E^{\mathrm{eff}}}\sigma_{ij} - \frac{\nu^{\mathrm{eff}}}{E^{\mathrm{eff}}}\sigma_{kk}\delta_{ij}, \tag{2}$$

where, as Robotnov has suggested [2]:

$$\begin{aligned} E^{\mathrm{eff}} &= E_0(1-\omega), \\ \nu^{\mathrm{eff}} &= \nu_0(1-\omega), \end{aligned} \tag{3}$$

where ν_0 and E_0 are respectively the Young and Poisson elastic moduli of a "vigin" material. The yield function depends on the linear invariant of σ_{ij} and the quadric invariant of σ_{ij}. The model involves two variables of state: the equivalent microscopic plastic strain, $\overline{\varepsilon}^{\mathrm{pl}}$, and ω, definied as volume fraction of voids. The yield surface is of the following form [7]:

$$\Phi(q,p,\overline{\varepsilon}^{\mathrm{pl}},\omega) = \left(\frac{q}{\sigma_y}\right)^2 - 2\omega\cosh\left(\frac{-3p}{2\sigma_y}\right) - \left(1+\omega^2\right) = 0, \tag{4}$$

where $q = \sqrt{\frac{3}{2}S_{ij}S_{ij}}$ is the Huber-Mises equivalent stress, S_{ij} is the deviatoric part of σ_{ij}, $p = -\sigma_{kk}/3$ is hydrostatic stress and σ_y is the flow stress of the matrix material. The yield function is used as the plastic potential, so that:

$$\dot{\varepsilon}_{ij} = \dot{\lambda}\frac{\partial\Phi}{\partial\sigma_{ij}} = \frac{\dot{\lambda}}{\sigma_y}\left[\frac{3S_{ij}}{\sigma_y} - \omega\sinh\left(\frac{3p}{2\sigma_y}\right)\delta_{ij}\right]. \tag{5}$$

The evolution equation for variable $\overline{\varepsilon}^{\mathrm{pl}}$ is based on the requirement that macroscopic plastic work $\sigma_{ij} : \dot{\varepsilon}_{ij}^{\mathrm{pl}}$ equals $(1-\omega)\sigma_y\overline{\varepsilon}^{\mathrm{pl}}$, so:

$$\overline{\varepsilon}^{\mathrm{pl}} = \frac{\sigma_{ij} : \dot{\varepsilon}_{ij}^{\mathrm{pl}}}{(1-\omega)\sigma_y}. \tag{6}$$

As a porous metal deforms plastically, its porosity may change due to the growth or closure of the existing voids or nucleation of new voids:

$$\dot{\omega} = \dot{\omega}_{gr} + \dot{\omega}_{ini}. \tag{7}$$

Assuming that the cristal material is plastically incompressible, it can readily be demonstrated that:

$$\dot{\omega}_{gr} = (1-\omega)\dot{\varepsilon}_{kk}^{\mathrm{pl}}. \tag{8}$$

We consider plastic strain-controlled nucleation such that:

$$\dot{\omega}_{ini} = \mathscr{A}\,\dot{\overline{\varepsilon}}_m^{\mathrm{pl}}, \tag{9}$$

where, as suggested in [17], parameter $\mathscr{A}$ is so chosen that the nucleation strain follows a normal distribution with mean value ε_N and standard deviation S_N:

$$\mathscr{A} = \frac{f_N}{S_N\sqrt{2\pi}}\exp\left[-\frac{1}{2}\left(\frac{\overline{\varepsilon}_m^{\mathrm{pl}} - \varepsilon_N}{S_N}\right)^2\right], \tag{10}$$

f_N being the volume fraction of void-nucleating particles.

2.2. Mass transport in metal

Let us formulate the general problem for chemical compound transport in metal as follows:

$$\frac{dc^k}{dt} = \nabla \cdot \left(D^k \nabla c^k \right) + S_c^k , \tag{11}$$

where c^k is a concetration of k^{th} chemical compound in metal, D^k is the diffusion coefficient tensor of a given corrosive factor and S_c^k is the source. In our model the diffusion coefficient tensor is a function of total strain and local damage:

$$D_{ij}^k = D^{k,0} \exp\left(\frac{-Q^k}{RT} \right) A^{k,1} \varepsilon_{ij}^{\text{tot}} + \omega D_\omega^0 \exp\left(\frac{-Q_\omega}{RT} \right) \delta_{ij} , \tag{12}$$

where Q^k and Q_ω are activation energies of a given chemical compound and damage, $A^{k,1}$ is the material constant for steel and the chemical compound, T is temperature and R – the gas constant. Now the model includes an extension of the damage evolution equation (7):

$$\dot{\omega} = \dot{\omega}_{\text{gr}} + \dot{\omega}_{\text{ini}} + \dot{\omega}_{\text{chem}} , \tag{13}$$

where $\dot{\omega}_{\text{chem}}$ is the source of damage due to the concentration of a given chemical compound:

$$\dot{\omega}_{\text{chem}} = \sum_{k=1}^{n} A^k c_k \exp\left(c^{\text{H}_2\text{O}} \right), \tag{14}$$

A_5^k being a material constant and c_k the concentration of a given chemical compound.

3. Numerical examples

The model contains many material constants, so the first step in their calibration should be a comparison of numerical and experimental data of steel samples under external mechanical force in ambient (*e.g.* air) and corrosion environment.

3.1. Sample in air

First, a comparison was made of experimental and numerical results for a sample in air.

Table 1. Material constants for 34CrAlNi7 steel; $q = 1.5$ value taken from [18] and [19]

n	b	f_N	ϵ_N	s_N	q
4.03	501.3	0.003	0.29	0.09	1.5

Exemplary results of Huber-Mises stress taken from calibration tests are shown in Figures 1 and 2. A comparison of experimental and calculated strain-force curves for material parameters taken from Table 1 is presented in Figure 3 with quite good compatibility. In Figure 4, a normalized Huber-Mises stress and damage parameter ω is presented versus global strain for five areas of the sample's cross-section at half length; the value of stress decreases with increasing value of damage parameter. The same effect is presented in Figures 5 and 6, taken from point "D" in Figure 4.

3.2. Sample in H_2SO_4

Further calculations were performed for the same sample filled in H_2SO_4, starting with calculations of the aggressive compound's concentration. The initial

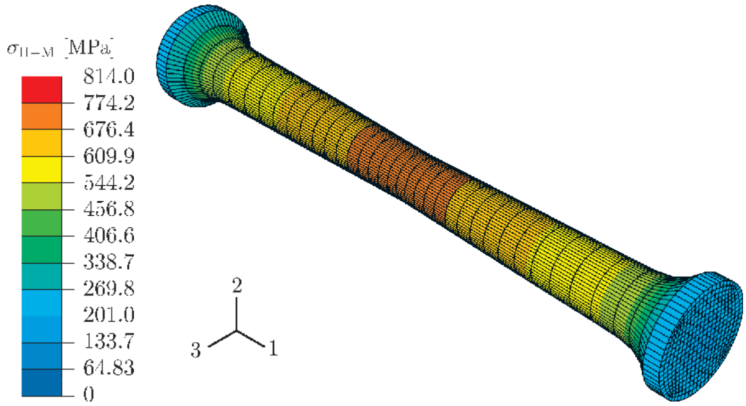

Figure 1. Example of calculations: Huber-Mises stress in a sample, point "B" in Figure 4

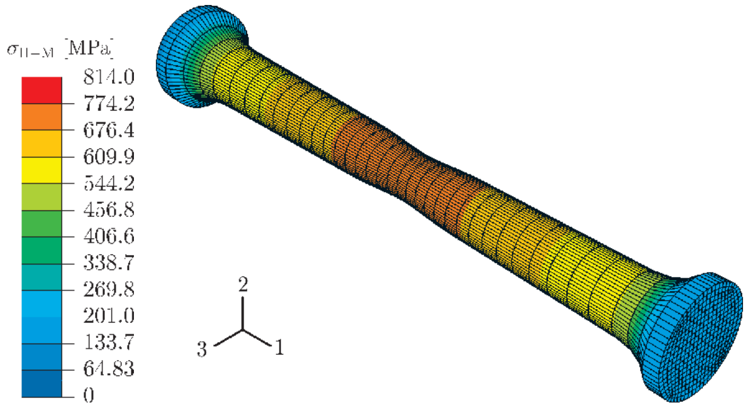

Figure 2. Example of calculations: Huber-Mises stress in a sample, point "D" in Figure 4

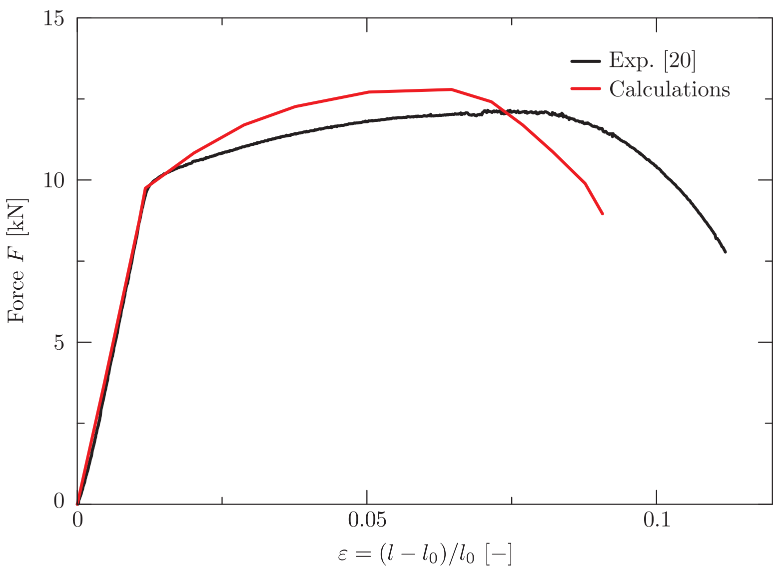

Figure 3. Results of comparison of numerical and experimental strain-force curves, sample in air

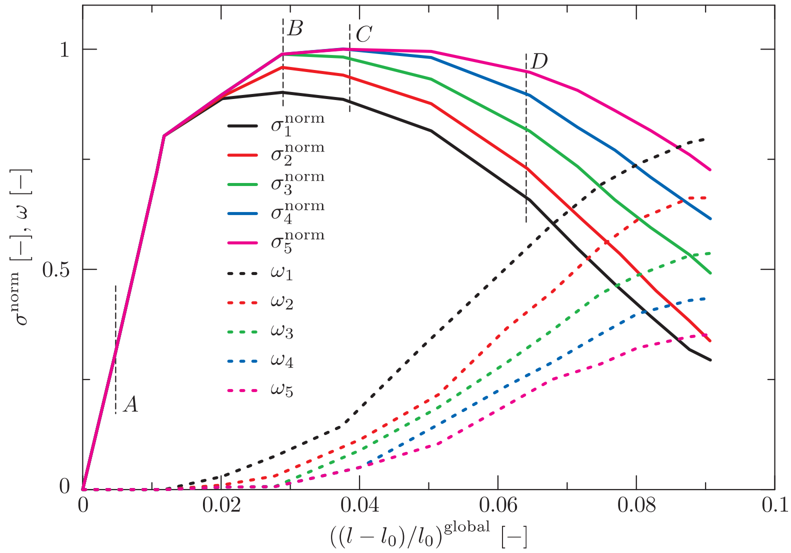

Figure 4. Normalized stress and damage parameter versus strain, results of calculations

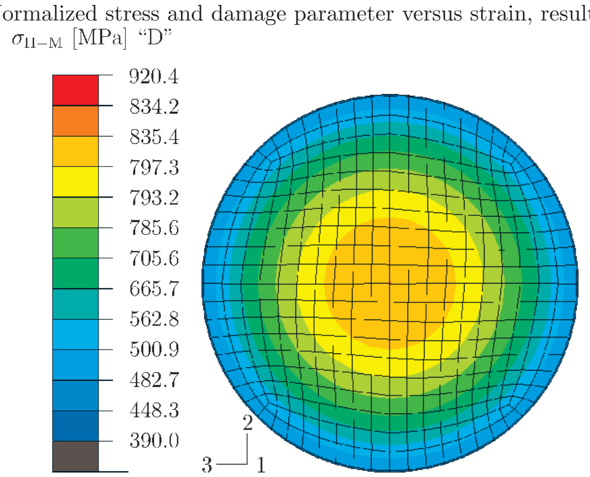

Figure 5. Huber-Mises stress at the sample's cross-section at half length, at point "D" in Figure 4

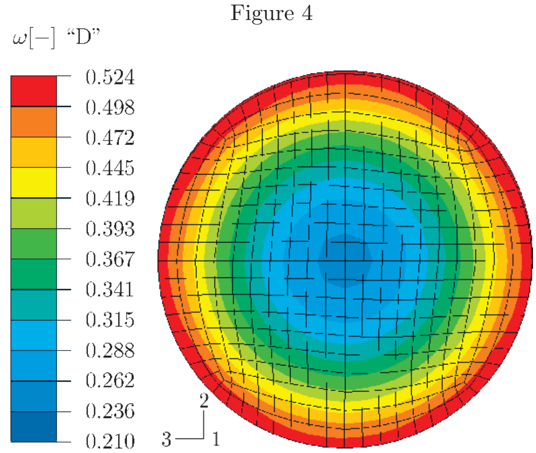

Figure 6. Damage parameter ω at the sample's cross-section at half length

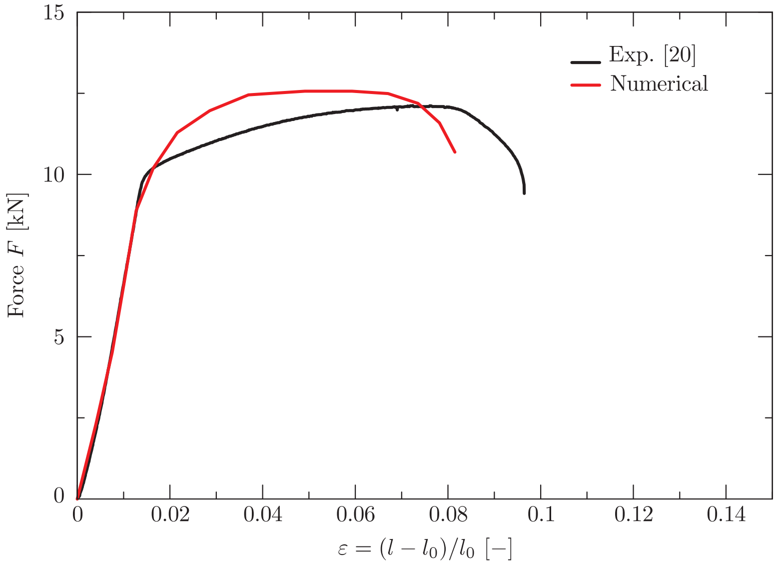

Figure 7. Results of comparison of numerical and experimental strain-force curves, sample in H_2SO_4

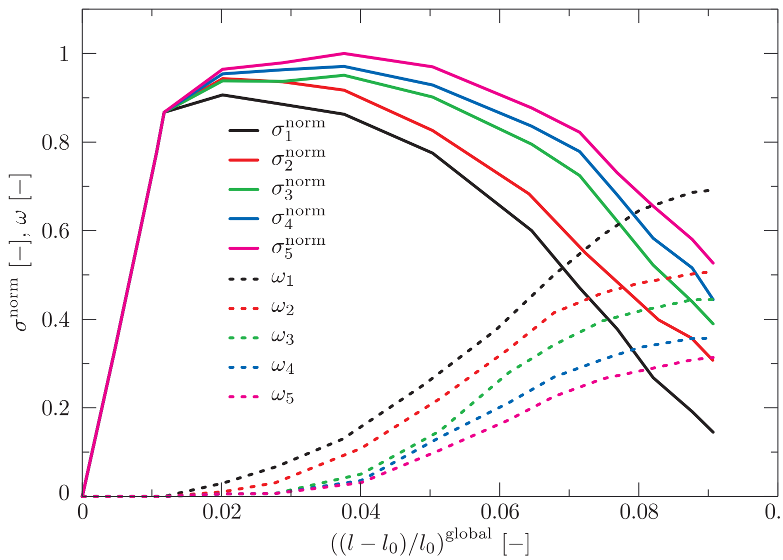

Figure 8. Normalized stress and damage parameter versus strain, results of calculations for H_2SO_4 environment

concentration of hydrogen at the sample's boundary surface can be calculated from the hydrolysis reaction of H_2SO_4:

$$\underset{98\,\mathrm{g}}{\overset{0.01\,\mathrm{M}}{\mathrm{H_2SO_4}}} \overset{\mathrm{H_2O}}{\longleftrightarrow} \underset{2\,\mathrm{g}}{\overset{x}{2\mathrm{H}^+}} + \mathrm{SO}_4^-, \quad \text{so} \quad x = 2.04 \cdot 10^{-4}\,\mathrm{M}. \tag{15}$$

As in the previous case, comparison of experimental and numerical strain-force curves obtained for material parameters from Table 2 is presented in Figure 7. Normalized Huber-Mises stress versus strain is presented in Figure 8 and exhibits

Table 2. Model constants for 34CrAlNi8 steel; $q = 1.5$ value taken from [18, 19]

n	b	f_N	ϵ_N	s_N	q	c_0	A^{tot}
3.81	487.4	0.003	0.29	0.09	1.5	$2.04 \cdot 10^{-4}$	0.48

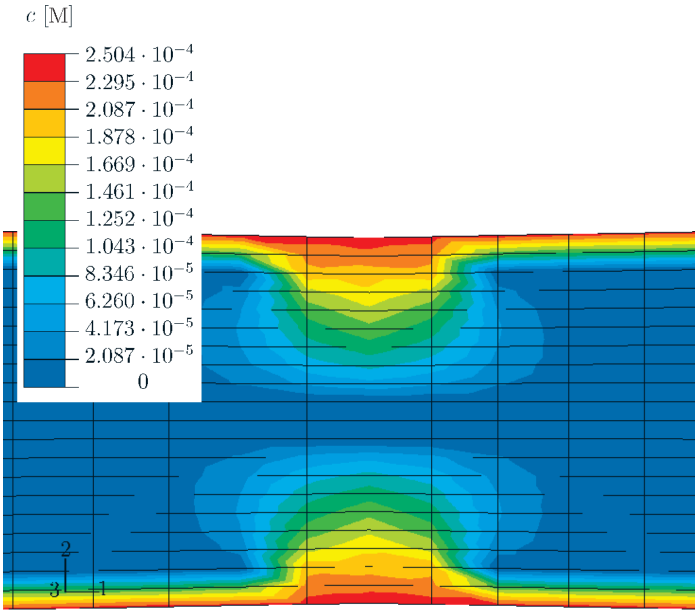

Figure 9. Sample results of corrosive factor's (H^+) penetration into metal ($\varepsilon = 0.026$)

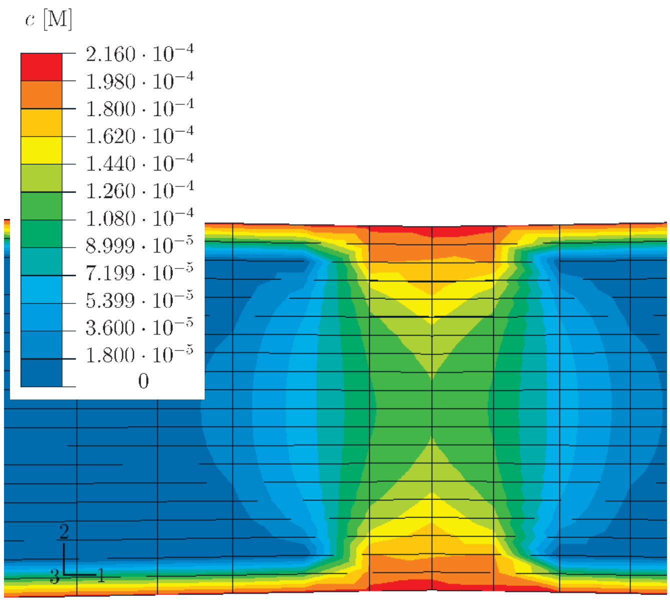

Figure 10. Sample results of corrosive factor's (H^+) penetration into metal ($\varepsilon = 0.062$)

the same effect as that presented in the previous subsection. Figures 9 and 10 present stress diffusion of hydrogen for two elongations $\varepsilon = 0.026$ and $\varepsilon = 0.062$.

4. Conclusions

- The present paper is a compilation of ideas of CDM (effective elastic moduli), Gurson's yield function with Needleman extension and Fick's law, and describes ductile damage of steel samples in an aggressive environment. A comparison of experimental and numerical $F-\varepsilon$ is presented in Figures 3 and 7.
- The proposed mechanism of coupling between the stress state and mass transport yields similar results as that given by Yokobori [20]. It means that the concentration of hydrogen in the place where the material is stressed is higher and it penetrates the metal more intensely (Figures 9 and 10).
- A simple form of the equation for damage from the presence of chemical compounds (Equation (14)) is good enough to describe the influence of a corrosive factor.

Acknowledgements

This work has been supported by the State Committee of Scientific Research (KBN) under contract no. 1303/T10/2005/28.

References

[1] Mudry F 1987 *A local approach to cleavage fracture*, *Nucl. Eng. Design* **105** 65
[2] Norton F H 1929 *The Creep of Steel at High Temperature*, McGraw-Hill
[3] Almroth P, Hasselqvist M, Sjostrom S and Simonsson K 2002 *Modeling of the high temperature behaviour of IN792 in gas turbine hot parts*, *Comput. Mat. Sci.* **25** 305
[4] Bielecki M 2000 *Numerical Modelling of Damage of Termomechanically Loaded Materials*, PhD Thesis, IMP PAN (in Polish)
[5] Becker A A, Hyde T H, Sun W and Andersson P 2002 *Benchmarks for finite element analysis of creep continuum damage mechanics*, *Comput. Mat. Sci.* **25** 34
[6] Rice J R and Tracy D M 1969 *On ductile enlargement of voids in triaxial stress fields*, *J. Mech. Phys. Solids* **17** 210
[7] Gurson A L 1977 *Continuum theory of ductile rupture by void nucleation and growth: Part I – yield criteria and flow rules for porous ductile media*, *J. Eng. Mater. Technol.* **99** 2
[8] Needleman A and Rice J R 1978 *Limits to Ductility Set by Plastic Flow Localization*, Mechanics of Sheet Metal Forming, Plenum Press
[9] Nishimura R and Meada Y 2004 *Scc evaluation of type 304 and 316 austenitic stainless steels in acidic chloride solutions using the slow strain rate technique*, *Corrosion Sci.* **46** 343 – 360
[10] Nishimura R, Daisuke S and Meada Y 2004 *Hydrogen permeation and corrosion behavior of high strength steel mcm 430 in cyclic wet-dry SO_2 environment*, *Corrosion Sci.* **46** 225
[11] Tokei Z, Viefhaus H and Grabke H J 1997 *High temperature oxidation of Fe-Cr alloys in wet oxygen*, *Oxid. Met.* **48** 198 – 212
[12] Gree A P, Louw C W and Swart H C 2000 *The oxidation of industrial FeCrMo steel*, *Corrosion Sci.* **42** 1725
[13] Ostwald C and Grabke H J 2004 *Initial oxidation and chromium diffusion. I: effects of surface working on 9–20% Cr steels*, *Corrosion Sci.* **46** 1113
[14] Kucharski R 2003 *Stress Corossion Damage of Inelastic Strained Material*, Intern. rep. IMP-PAN nr 3839/03, pp. 1–16 (in Polish)
[15] Kucharski R 2003 *No-load Corrosion*, Intern. rep. IMP-PAN nr 3838/03, pp. 1–10 (in Polish)

[16] Badur J, Karcz M, Kowalczyk S, Lemański M and Kucharski R 2004 *Analysis of Temperature Field Anomaly in Gas Turbine GT8C*, Intern. rep. IMP-PAN nr 4110/04, Gdansk, pp. 1–26 (in Polish)

[17] Chu C C and Needleman A 1980 *Void nucleation effecs in biaxially stretched sheets*, *Int. J. Eng. Mat. Technol.* **102** 249

[18] Ramaswamy S and Aravas N 1998 *Finite element implementation of gradient plasticy models. Part I: Gradient-dependent yield functions*, *Computer Meth. Appl. Mech. Eng.* **163** 11

[19] Ramaswamy S, Aravas N 1998 *Finite element implementation of gradient plasticy models. Part II: Gradient-dependent evolution equations*, *Computer Meth. Appl. Mech. Eng.* **163** 33

[20] Yokobori A T 2004 *The mechanism of hydrogen embrittlement: the stress interaction between a crack, a hydrogen cluster, and moving dislocations*, *Int. J. Fracture* **128** 121